

Dear Editor,

First of all on behalf of all co-authors, I would like to thank the reviewers for their helpful comments and suggestions. I believe that we have successfully integrated all the reviewers' comments and requests, and that these changes have greatly improved the manuscript. Please find the revised version of our manuscript cp-2015-94.

Briefly, the text has been revised taking into account the reviewers comments. In addition, all figures were modified following the suggestions of the reviewers.

I look forward to hearing from you and if you have any further queries please do not hesitate to contact me.

Yours sincerely,

Bassem Jalali

# Holocene climate variability in the North-Western Mediterranean Sea (Gulf of Lions)

Jalali B.<sup>1,2</sup>, M.-A. Sicre<sup>2</sup>, M.-A. Bassetti<sup>3</sup>, and N. Kallel<sup>1</sup>

<sup>1</sup>GEOGLOB, Université de Sfax, Faculté des Sciences de Sfax, route de Soukra km 4-BP.802, 3038, Sfax, Tunisia.

<sup>2</sup>Sorbonne Universités (UPMC, Université Paris 06)-CNRS-IRD-MNHN, LOCEAN Laboratory, 4 place Jussieu, F-75005 Paris, France.

<sup>3</sup>CEFREM, Université de Perpignan, Avenue J.-P. Alduy, 66860 Perpignan, France.

## Abstract

Sea surface temperatures (SSTs) and land-derived input time series were generated from the Gulf of Lions inner-shelf sediments (NW Mediterranean Sea) using alkenones and high-molecular-weight odd-carbon numbered *n*-alkanes (TERR-alkanes), respectively. The SST record depicts three main phases: a warm Early Holocene ( $\sim 18 \pm 0.4^\circ\text{C}$ ) followed by a cooling of  $\sim 3^\circ\text{C}$  between 7000 and 1000 BP, and rapid warming from  $\sim 1850$  AD onwards. Several superimposed multi-decadal to centennial scale cold events of  $\sim 1^\circ\text{C}$  amplitude were also identified. TERR-alkanes were quantified in the same sedimentary horizons to identify periods of high Rhone River discharge and compare them with regional flood reconstructions. Concentrations show a broad increase from the early Holocene towards present with a pronounced minimum around 2500 BP and large fluctuations during the second part of the Holocene. Comparison with Holocene flood activity reconstructions across the Alps region suggests that sediments of the inner shelf originate mainly from the Upper Rhone River catchment basin and that they are primarily delivered during positive North Atlantic Oscillation (NAO).

## 1 Introduction

Several proxy records have documented surface water variability of the Mediterranean Sea during the Holocene (Kallel et al., 1997a,b, 2004; Cacho et al., 2001; Guinta et al., 2001; Rohling et al., 2002; Emeis et al., 2003; Essalami et al., 2007; Frigola et al., 2007; Castañeda et al., 2010; Boussetta et al., 2012; Martrat et al., 2014). Most of them reveal that Mediterranean Sea surface temperatures (SSTs) have undergone a long-term cooling punctuated by several cold relapses (CRs) (Cacho et al., 2001; Frigola et al., 2007). While orbital forcing likely explain this long-term tendency, solar activity and volcanism contribute to

36 forced variability (Mayewski et al., 2004; Wanner et al., 2011) together with internal variability  
37 (i.e. Atlantic Multi-decadal variability (AMV), North Atlantic Oscillation (NAO)...) all together  
38 embedded in the observed multi-decadal scale variability seen in paleorecords. Josey et al.  
39 (2011) have shown that the East Atlantic pattern (EA) and the NAO are the most important  
40 modes of atmospheric variability influencing heat loss and convection in the Mediterranean  
41 basin. For example, cold intense winds closely related to negative EA and NAO would have  
42 triggered the severe coldness and deep convection in winter 2004/05 and 2005/06 in the Gulf  
43 of Lions (Schroeder et al., 2011). Owing to this tight link with the large-scale atmospheric  
44 circulation (Josey et al., 2011) annual SSTs in the Gulf of Lions are colder than the annual  
45 mean for the whole Mediterranean basin due to surface water heat loss caused by Mistral  
46 and Tramontane winds (Fig. 1). The Tramontane originates from the northwest blowing  
47 through the Naurouze passage, while Mistral winds are northerly winds channeled by the  
48 Rhone river valley that causes convection in the Gulf of Lions (Auclair et al., 2000). Indeed,  
49 dense waters form over the continental shelf upon winter cooling by strong Mistral and then  
50 spread downslope to the abyssal plain. This cascading of dense waters contributes to open  
51 ocean deep convection but the main mechanism leading to the formation of Western  
52 Mediterranean Deep Water (WMDW) is open sea convection (Béthoux et al., 2002). In that  
53 case, Mistral initiates vertical mixing till the surface mixed layer reaches the underlying saltier  
54 Levantine Intermediate Water (LIW), and upon buoyancy loss triggers deep convection  
55 (Schroeder et al., 2010). The heat and salt contents of the LIW together with wind strength  
56 are thus the main factors controlling deep convection in the Gulf of Lions (Schroeder et al.,  
57 2011).

58 Atmospheric circulation is also important to the hydrological budget of the Mediterranean  
59 Sea. Rainfall in the NW Mediterranean Sea mainly occurs in winter (October to March) and is  
60 very much reliant on the position of the storm tracks and strength of NAO (Hurrell et al.,  
61 2003). Indeed, during negative NAO, their southerly position results in enhanced winter  
62 rainfall over the Southern Europe and the NW Mediterranean Sea while at high NAO storm  
63 trajectories are shifted to the North and precipitations are more intense in Northern Europe.  
64 Changes in the mid-latitude atmospheric circulation in the North Atlantic are thus expected to  
65 impact on the Rhone River flow during the Holocene. Most of the precipitation occurs in  
66 autumn and contribute through different tributaries to the water discharge of the Rhone River.  
67 The upper Rhone River catchment basin receives precipitations originating from the North  
68 Atlantic along the year while from the Southern Lower Rhone tributaries are affected by  
69 extreme rainfalls in September and October due to inland penetration of maritime southerly  
70 winds. These heavy rain episodes in southern France result in intense floods causing  
71 important damages. The water and solid discharges of the Rhone River are thus highly

72 seasonal. About 80% of the sediments of the Gulf of Lions continental shelf is supplied by  
73 the Rhone River giving rise to high sedimentation rates in this area (Aloïsi et al., 1977).  
74 Indeed, the surface circulation in the Gulf of Lions is characterized by the geostrophic North  
75 Current flowing along the continental slope from the Ligurian to the Catalan basins (Millot,  
76 1999). Along its path, the North Current receives freshwater and suspended matter mostly  
77 from the Rhone River. In the inner shelf, the westward coastal flow advects the Rhone river  
78 plume suspended particles, settling as a wedge-shaped body and defining as mud belt  
79 (Cattaneo et al., 2003; Bassetti et al., 2015).

80 In this study, we produced a high-resolution SST record of the past 10 000 years from the  
81 high accumulation rate of the Gulf of Lions shelf sediments based on alkenone  
82 paleothermometry to document past changes of surface water heat content and their link  
83 with atmospheric circulation. TERR-alkanes were determined in the same sediment horizons  
84 to assess land-derived inputs from the Rhone River and identify flood periods and their  
85 relationship with the long-term and multi-decadal variability of SSTs.

86

## 87 **2. Material and methods**

88 Both a gravity core (KSGC-31) and multi-core (GolHo-1B) were retrieved from virtually the  
89 same site in the Rhone mud belt deposited onto the Gulf of Lions inner-shelf (43°0'23"N;  
90 3°17'56"E, water depth 60 m) (Fig. 1). The 7 meter long gravity core KSGC-31 was  
91 recovered during the GM02-Carnac cruise in 2002 on the R/V *Le Suroît*, while the 20 cm  
92 long multi-core GolHo-1B was collected during the GolHo cruise in 2013, on the R/V *Nerys*.  
93 Both sediment cores were sliced continuously at a sampling step of 1 cm for biomarker  
94 analyses.

### 95 **2.1. Core chronology**

96 The age model of the gravity core KSGC-31 is based on 21 radiocarbon dates obtained by  
97 Accelerator Mass Spectrometry (AMS) performed by the Laboratoire de Mesure du Carbone  
98 14 (Saclay, France) and in the Beta Analytic Radiocarbon Dating Laboratory (Florida, USA)  
99 (Table 1). The two uppermost dates indicate post-bomb values. The <sup>14</sup>C dates were  
100 converted into 1 calendar years using Calib7.1 (Stuiver and Reimer, 1993) and the  
101 MARINE 13 calibration dataset with a reservoir effect of 400 yrs (Reimer et al., 2013) (Table  
102 1). We used a local marine reservoir age of  $R = 23 \pm 71$  years as an additional correction  
103 (<http://calib.qub.ac.uk/marine/regioncalc.php>). The age model was obtained by linear  
104 interpolation between <sup>14</sup>C dates excluding the minor reversal at 18.5 cm (350 ± 78 yr). The  
105 age control for the upper portion of the core is based on <sup>210</sup>Pb profile measured in the upper  
106 10 cm of KSGC-31 spliced with the <sup>210</sup>Pb profile of the GolHo-1B multi-core. Based on the  
107 <sup>210</sup>Pb chronology, the age of the gravity KSGC-31 core-top was estimated to be approx. 1971

108 ± 1.4 yr AD. The GolHo-1B multi-core, spanning a range from 1960 ± 5.6 to 2013 yr AD, thus  
109 extends the SST record to present day. The two upper post-bomb radiocarbon ages  
110 converted using OxCal 4.2 (Ramsey and Lee, 2013) are in good agreement with the <sup>210</sup>Pb  
111 chronology (Table 1). Details on the age model description for the past 2000 yr as well as on  
112 splicing GolHo-1B and upper part of KSGC-31 records can be found in Sicre et al. (in  
113 revision). The obtained spliced KSGC-31\_GolHo-1B SST signal presented here covers the  
114 past 10000 years, including the 20<sup>th</sup> century. The mean sedimentation rate is ~ 80 cm (1000  
115 yr)<sup>-1</sup>.

## 116 2.2. Biomarker analyses

117 Lipids were extracted from 2 to 3 grams of freeze-dried sediments using a mixture of (3:1 v/v)  
118 dichloromethane/methanol. We performed continuous sampling of the cores at a sampling  
119 step of 1 cm (i.e. over 700 samples) which based on our age model translate to a mean  
120 temporal resolution of ca. 15 yrs. Alkenones and *n*-alkanes were isolated for the total lipid  
121 extract by silica gel chromatography and quantified by gas chromatography as described by  
122 Ternois et al. (1996). The global calibration published by Conte et al. (2006) was used to  
123 convert the unsaturation ratio of C<sub>37</sub> alkenones ( $U_{37}^k = C_{37:2}/(C_{37:2} + C_{37:3})$ ) to SSTs ( $T (^{\circ}C) = -$   
124  $0.957 + 54.293(U_{37}^k) - 52.894(U_{37}^k)^2 + 28.321(U_{37}^k)^3$ ) into production temperatures. External  
125 precision using this calibration has been estimated to be ± 1.2 °C while analytical precision  
126 after triplicate injections is less than 0.01 U<sub>37</sub><sup>k</sup> unit ratio, which, in the temperature range of  
127 our data, translates into ± 0.3°C.

128 N-alkane concentrations were calculated using 5α-cholestane as an external standard. Only  
129 the high-molecular-weight n-alkanes with an odd carbon number, i.e. C27+C29+C31+C33  
130 homologs (hereafter TERR-alkanes), were quantified to track land-derived inputs. These  
131 compounds are primarily synthesized by higher plants and are constituents of epicuticular  
132 waxes of leaves. Their accumulation in the sediments of Gulf of Lions is primarily associated  
133 with the discharge and deposition of the Rhone River suspended particles in relation with  
134 precipitations (Ludwig et al., 2010).

135

## 136 3. Results

137 Figure 2a shows the temporal evolution of SSTs at the KSGC-31\_GolHo-1B site over the  
138 past 10000 years, including the post-industrial period. The data indicate warm values of  
139 about 18±0.4°C between ca. 10000 to 7000 yr BP followed by a long-term cooling starting ~  
140 7000 yr BP culminating during the Dark Ages (DA) and a post-industrial warming that does  
141 not reach values as high as those of the Early Holocene (10000-7000 yr BP). Several multi-

142 decadal to multi-centennial scale CRs on average cooler by ~ 1°C (grey bars in Fig. 2) are  
143 superimposed on these trends (Table 2).

144 TERR-alkanes are used to assess terrestrial inputs from the Rhone River and their possible  
145 link to flood events and large-scale precipitation patterns (Fig. 2b). Concentrations range  
146 from 300 to 1800 ng g<sup>-1</sup> with lowest values during the early Holocene increasing from ~7000  
147 yr BP to present, except for a pronounced drop centered at ~ 2500 BP. They also show large  
148 multi-centennial fluctuations mostly during the second half of the Holocene (from ~6000 yr  
149 BP to present) with highest values during the Common Era (past 2000 yr) maximizing during  
150 the Medieval Climate Anomaly (MCA; 900-1300 yr AD), and a decrease over the last  
151 century. Seven multi-centennial scale time intervals of high TERR-alkane (HTE) were  
152 identified during the past 6000 yr (Table 3). HTE were defined as the time span where values  
153 exceeded one half of the standard deviation of the Holocene mean value after applying a 60  
154 yr FFT smoothing of the data.

155 In the following section we compare our SST record to earlier published time series from the  
156 Western and Eastern Mediterranean basins. We also discuss the Gulf of Lions TERR-alkane  
157 record in relation with flood reconstructions from the Northern and Southern Alps (Wirth et  
158 al., 2013) and Bourget Lake sediments located in the Upper Rhone River catchment basin  
159 (Arnaud et al., 2012) to infer additional information on atmospheric circulation regime.

160

## 161 4. Discussion

### 162 4.1. General trends

163 The temporal evolution of SSTs in the Gulf of Lions depicts three main phases. A warm Early  
164 Holocene at the time of high summer insolation in the northern Hemisphere, ending by cold  
165 event, CR1 (6600-5750 BP). Thereafter, SSTs show a general decline till about 1000 BP  
166 with notable cold intervals (CR2 to CR6) and a post-industrial warming. Our record shows  
167 strong similarities with the recent world-wide compilation of 73 marine records of Marcott et  
168 al. (2013) exhibiting a warm plateau between 10000 and 5000 yr BP and a 0.7°C cooling  
169 from 5500 to 100 yr BP in the extratropical Northern Hemisphere (30° to 90°N). The 2.5 °C  
170 cooling calculated from our record between 7000 and 100 yr BP is comparable to the 2°C  
171 decrease calculated by Marcott et al. (2013) in the high-latitude North Atlantic, outlying the  
172 influence of the Atlantic climate on the Mediterranean SSTs. Note that cooling in the Gulf of  
173 Lions is steeper (~3 °C) when calculated from 7000 to 1000 BP.

174 Figure 3 compares our results with Mediterranean SST published reconstructions (Table 4).  
175 Except for the MD99-2343 ( $\delta^{18}\text{O}$  of *G. bulloides*) and GeoB7702-3 cores (TEX86)  
176 (Castañeda et al., 2010), these reconstructions are all based on alkenone paleothermometry.

177 Owing to [their](#) age uncertainties and low temporal resolution, only trends and centennial to  
178 millennial-scale variability of the climate signals are retained and will be discussed here.  
179 Comparison of these regional time-series [reveals rising and generally warmer SSTs in all](#)  
180 [records between ca. 10 000 and 7000 yrs BP. Thereafter, differences are notable](#) between  
181 the Western and Eastern Mediterranean basins. In particular, the Alboran, the Balearic  
182 Islands, [and the](#) Gulf of Lions records all show a marked cooling through the middle to late  
183 Holocene. This is also the case in the central Mediterranean (Adriatic, Southern Tyrrhenian  
184 and Ionian seas), while SSTs in the Levantine basin indicate no or slight warming. This W-E  
185 evolution of Holocene SSTs [highlights](#) common features of the mid-latitude North Atlantic  
186 and NW Mediterranean that are distinct from the SE Mediterranean. [The long-term SST](#)  
187 [decrease in the North Atlantic and Western Mediterranean and concomitant increase in the](#)  
188 [Eastern Mediterranean Sea is in agreement with the findings of Rimbu et al. \(2003\) and their](#)  
189 [hypothesis of a long-term weakening of NAO over the Holocene due to tropical warming in](#)  
190 [winter as a result of increase low latitude insolation.](#)

#### 191 **4.2. North-western Mediterranean CRs**

192 Six CRs of different duration and amplitude were identified in Gulf of Lions SST record ([Table](#)  
193 [2](#)). The occurrence of CRs has been previously described in global compilations (Mayewski  
194 et al., 2004; Wanner et al., 2011) and seems to be associated with glacier advances in  
195 Europe (Denton and Karlén, 1973). They reflect either polar cooling or tropical aridity and  
196 likely express atmospheric circulation changes (Mayewski et al., 2004). The influence of the  
197 AMV has also been suggested (Kushnir and Stein, 2010). There are, however, discrepancies  
198 on the spatio-temporal distribution and amplitude of these events (Wanner et al., 2011,  
199 2014). Each CR does not necessarily impact everywhere with the same intensity due to local  
200 responses to climate changes. The sensitivity of proxies or particular sediment settings (e.g.  
201 coastal areas), their seasonal character, may also be another reason for not detecting CRs in  
202 all records. For example, it is interesting to note that the 8200 yr BP, well expressed in  
203 Greenland ice cores ([Johnsen et al., 2001](#)) is not found in the core KSGC-31\_GolHo-1B  
204 despite the high temporal resolution of this record ([Fig. 2](#)). When present in the extratropics,  
205 these short-term coolings have been attributed to strong cold and dry winds blowing from the  
206 North possibly triggered by a slowdown of the thermohaline circulation in the North Atlantic  
207 (Mayewski et al., 2004).

208 According to Kushnir and Stein (2010), cold SSTs in the tropical Atlantic would cause the  
209 formation of a high-pressure over the Eastern Atlantic extending towards Western Europe  
210 and the W-Mediterranean Sea similar to EA. This large-scale atmospheric pattern would  
211 impact on [temperature](#) and precipitations in the Mediterranean region as far as in the Levant  
212 region. Intensified northerly winds during the CR thus likely reinforced convection in the Gulf

213 of Lions by surface cooling (Schroeder et al., 2008; Josey et al., 2011). The study of the  
214 Minorca drift sediment (MD99-2343 core, Frigola et al., 2007) suggest that grain size in this  
215 area provides a record of bottom current vigor presumably induced by deep-water convection  
216 in the Gulf of Lions. To address this issue, we compared the % of non-carbonate fraction >10  
217  $\mu\text{m}$  (UP10) of the Minorca core to our SST reconstruction. As can be seen from Fig. 2a and c  
218 most of the CRs of the Gulf of Lions seem to correspond to higher values of UP10. This is  
219 less obvious prior 7000 yr BP and for shorter events when age model uncertainties become  
220 limiting for definite conclusions. Synchronicity between episodes of intensified upwelling in  
221 the Alboran Sea and high UP10 values at Minorca has also been discussed by Ausin et al.  
222 (2015) and explained by NAO. Based on the good match between UP10 values and the NAO  
223 index reconstruction of Olsen et al. (2012), these authors put forwards the hypothesis that  
224 persistent negative NAO would have triggered both stronger upwelling in the Alboran Sea  
225 and northerly wind induced convection over the Gulf of Lions, yet alkenone SSTs in their  
226 record do not show surface water cold events. The absence of cooling in KSGC-31\_GolHo-  
227 1B at the time of M8 and M7 events is also notable and suggests that Mistral was either  
228 weaker or did not affect the Gulf of Lions inner shelf area, while offshore deep convection  
229 would have been taken place. However, Frigola et al. (2007) also pointed out the equivocal  
230 relationship between M events and geochemical tracers in the Balearic records as for  
231 example with the  $\delta^{18}\text{O}$  of *G. bulloides*, even though not a pure temperature proxy. All  
232 together, these mismatches between SSTs and M events suggest that a better  
233 understanding of the deep-water proxies and their link to SSTs is needed before any  
234 conclusion can be drawn on climatic causes of M events.

### 235 **4.3. Holocene flood activity**

236 We compared our record of TERR-alkanes to two regional reconstructions of flood intensity  
237 of the Northern and Southern Alps obtained from 15 lacustrine sediment cores (Wirth et al.  
238 2013) and the reconstruction of the Lake Bourget paleohydrology (Arnaud et al., 2012). As  
239 can be seen from Fig. 4, the generally lower TERR-alkane values between 10000 and 7000  
240 yr BP broadly coincide with lower hydrological activity in Lake Bourget, between 10000 -  
241 6000 yr BP (Fig. 4c). Thereafter, as SSTs indicate colder climate conditions (CRs) TERR-  
242 alkane exhibit high fluctuations (Fig. 2). During this period broadly coincident with the  
243 Neoglaciation, advances and retreats of the Alpine glaciers would have been responsible for  
244 these centennial scale variations (Schimmelpfennig et al., 2012). High TERR-alkanes in our  
245 record coincide with sediment flux increase in the Rhone delta plain (Provansal et al., 2003;  
246 Fanget et al., 2014) therefore indicating that TERR-alkane changes are not primarily linked to  
247 vegetation changes. Our results also indicate that TERR-alkane mainly reflect inputs from

248 the Northern tributaries of the Rhone River except between 4200 and 2800 yr BP time  
249 interval when high TERR-alkanes bear more resemblance with the low N-Alps flood record.

250 Lowest TERR-alkanes occurred during CR4, lying from 2500 and 2000 yr BP when flood  
251 activity in S-Alps was among the highest and NAO strongly negative (Fig. 4d). This finding  
252 has been explained by the more southerly position of the North Atlantic storm tracks leading  
253 to increase cyclogenesis and precipitations in the Mediterranean Sea (Schimmelpfennig et  
254 al., 2012) as expected from negative NAO (Trigo et al., 2000) affecting primarily the S-Alps,  
255 as hypothesized by Wirth et al. (2013). Low TERR-alkanes consistently reflect lower  
256 precipitation in the Rhone catchment due to weak influence of Westerly winds in the N-Alps  
257 Rhone tributaries. During the Common Era flood activity and changes in Rhone River  
258 discharge both increase but as discussed by Fanget et al. (2014), human activity, i.e. erosion  
259 due to land use, likely played a role in the overall increasing delivery of land derived material.

260

## 261 **5. Conclusions**

262 Alkenone-derived SSTs from core KSGC-31\_GolHo-1B provide a regional reconstruction of  
263 Holocene climate variability of the N-W Mediterranean. After a warm plateau between 10 000  
264 and 7000 yr BP, SSTs depict a cooling trend of 2.5°C from 7000 to 100 yr, comparable to the  
265 North Atlantic, primarily as a result of orbital forcing. The Late Holocene warming reversed  
266 this long-term cooling trend. Six CRs of different duration and amplitude were identified, with  
267 the notable exception for the 8200 yr event. Northerly and northwesterly winds blowing over  
268 the Gulf of Lions during negative NAO, and/or EA, are the most likely cause of these cold  
269 events.

270 TERR-alkanes accumulated in the inner shelf of the Gulf of Lions indicate low input during  
271 the early Holocene increasing a SSTs started to decline around ca. 6000 yr BP. Comparison  
272 with records of flood intensity from the Alps indicates that HTE primarily originate from the  
273 Upper Rhone River catchment basin, with possible contribution of the S-Alp tributaries  
274 between 4200 and 2800 yr BP. Lowest TERR-alkanes centered ~ 2500 years coincide with  
275 strongly negative NAO and cold SSTs when storms tracks had a most southerly position.  
276 This is when S-Alps floods were among the strongest. Our results highlight the complex and  
277 variable influence of the mid-latitude atmospheric circulation on the NW Mediterranean SSTs  
278 and precipitations on decadal to multi-decadal time scales over the Holocene.

279

## 280 **Acknowledgments**

281 We would like to thank MISTRALS/Paleomex for financial support and the crew operating the  
282 GMO2 Carnac (R/V "Le Suroît") and GolHo (R/V "Nerys") cruises. Nabil Sultan (GMO2

283 Carnac Chief Scientist) Serge Berné (IFREMER-CEFREM) and Bernard Dennielou  
284 (IFREMER) are thanked for giving access to the core KSGC-31 and to IFREMER laboratory  
285 facilities. The ARTEMIS programme is thanked for providing  $^{14}\text{C}$  from the Accelerator Mass  
286 Spectrometer located in Saclay, France (Laboratoire de Mesure du  $^{14}\text{C}$ ).  
287

- 289 Aloïsi, J. C., Auffret, G. A., Auffret, J. P., Barusseau, J. P., Hommeril, P., Larsonneur, C., Monaco, A.:  
290 Essai de modélisation de la sédimentation actuelle sur les plateaux continentaux français, *B. Soc.*  
291 *Geol. Fr.*, 19, 183–195, 1977.
- 292 Arnaud, F., Révillon, S., Debret, M., Revel, M., Chapron, E., Jacob, J., Giguet-Covex, C., Poulénard,  
293 J., and Magny, M.: Lake Bourget regional erosion patterns reconstruction reveals Holocene NW  
294 European Alps soil evolution and paleohydrology, *Quaternary Sci. Rev.*, 51, 81–92,  
295 doi:10.1016/j.quascirev.2012.07.025, 2012.
- 296 Auclair, F., Marsaleix, P., and Estournel, C.: Sigma coordinate pressure gradient errors: evaluation  
297 and reduction by an inverse method, *J. Atmos. Ocean. Tech.*, 17, 1348–1367, 2000.
- 298 Ausín, B., Flores, J. A., Sierro, F. J., Cacho, I., Hernández-Almeida, I., Martrat, B., and Grimalt, J. O.:  
299 Atmospheric patterns driving Holocene productivity in the Alboran Sea (Western Mediterranean): a  
300 multiproxy approach, *The Holocene*, 25, 1–13, doi:10.1177/0959683614565952, 2015.
- 301 Bassetti, M.-A., Berné, S., Sicre M.-A., Dennielou, B., Alonso, Y., Buscail R., Jalali, B., Hebert B.,  
302 Menniti, C.: Holocene hydrological changes of the Rhone River (NW Mediterranean) as recoded in  
303 the marine mud belt, *Clim. Past*, in preparation, 2015.
- 304 Béthoux, J.P., Durieu de Madron, X., Nyffeler, F., Tailliez, D.: Deep water in the western  
305 Mediterranean: peculiar 1999 and 2000 characteristics, shelf formation hypothesis, variability since  
306 1970 and geochemical inferences, *Journal of Marine Systems*, 33-34, 117-131, 2002.
- 307 Brown, M.: *Ocean Data View 4.0*, *Oceanography*, 11, 19–21, 1998.
- 308 Boussetta, S., Kallel, N., Bassinot, F.C., Labeyrie, L.D., Duplessy, J.-C., Caillon, N., Dewilde, F.,  
309 Rebaubier, H.: Mg/Ca-paleothermometry in the western Mediterranean Sea on planktonic  
310 foraminifer species *Globigerina bulloides*: Constraints and implications, *Comptes Rendus*  
311 *Geoscience*, 344, 267-276, 2012.
- 312 Cacho, I., Grimalt, J. O., Canals, M., Saffi, L., Shackleton, N., Schönfeld, J., and Zahn, R.: Variability  
313 of the western Mediterranean Sea surface temperature during the last 25 000 years and its  
314 connection with the Northern Hemisphere climatic changes, *Paleoceanography*, 16, 40–52, 2001.
- 315 Castañeda, I. S., Schefuß, E., Pätzold, J., Sinninghe Damsté, J. S., Weldeab, S., and Schouten, S.:  
316 Millennial-scale sea surface temperature changes in the eastern Mediterranean (Nile River Delta  
317 region) over the last 27 000 years, *Paleoceanography*, 25, PA1208, doi:10.1029/2009PA001740,  
318 2010.
- 319 Cattaneo, A. and Steel, R. J.: Transgressive deposits: a review of their variability, *Earth-Sci. Rev.*, 62,  
320 187–228, 2003.
- 321 Conte, M. H., Sicre, M.-A., Rühlemann, C., Weber, J. C., Schulte, S., Schulz-Bull, D., and Blanz, T.:  
322 Global temperature calibration of the alkenone unsaturation index (UK37) in surface waters and  
323 comparison with surface sediments, *Geochem. Geophys. Geosy.*, 7, Q02005,  
324 doi:10.1029/2005GC001054, 2006.
- 325 Denton, G. H. and Karlen, W.: Holocene climatic variations their pattern and possible cause,  
326 *Quaternary Res.*, 3, 155–205, 1973.
- 327 Emeis, K.-C., Struck, U., Schulz, H.-M., Bernasconi, S., Sakamoto, T., and Martinez-Ruiz, F.:  
328 Temperature and salinity of Mediterranean Sea surface waters over the last 16,000 years:  
329 constraints on the physical environment of S1 sapropel formation based on stable oxygen isotopes  
330 and alkenone unsaturation ratios, *Palaeogeogr. Palaeoclimatol.*, 158, 259–280, 2000.
- 331 Emeis, K. C., Struck, U., Blanz, T., Kohly, A., and Woß, M.: Salinity changes in the central Baltic Sea  
332 (NW Europe) over the last 10 000 years, *The Holocene* 13, 411–421, 2003.
- 333 Essallami, L., Sicre, M.-A., Kallel, N., Labeyrie, L., and Siani, G.: Hydrological changes in the  
334 Mediterranean Sea over the last 30 000 years, *Geochem. Geophys. Geosy.*, 8, Q07002,  
335 doi:10.1029/2007GC001587, 2007.
- 336 Fanget, A. S., Berné, S., Jouet, G., Bassetti, M.-A., Dennielou, B., Maillet, G. M., and Tondut, M.:  
337 Impact of relative sea level and rapid climate changes on the architecture and lithofacies of the  
338 Holocene Rhone subaqueous delta (Western Mediterranean Sea), *Sediment. Geol.*, 305, 35–53,  
339 doi:10.1016/j.sedgeo.2014.02.004, 2014.
- 340 Frigola, J., Moreno, A., Cacho, I., Sierro, F. J., Flores, J. A., Grimalt, J. O., Hodell, D. A., and Curtis, J.  
341 H.: Holocene climate variability in the western Mediterranean region from a deepwater sediment  
342 record, *Paleoceanography*, 22, PA2209, doi:10.1029/2006PA001307, 2007.

343 Giunta, S., Emeis, K. C., and Negri, A.: Sea-surface temperature reconstruction of the last 16 000  
344 years in the Eastern Mediterranean Sea, *Rivista Italiana di Paleontologia e Stratigrafia*, 107, 463–  
345 476, 2001.

346 Hurrell, J. W., Kushnir, Y., Ottersen, G., and Visbeck, M.: An overview of the North Atlantic Oscillation;  
347 The North Atlantic oscillation: climate significance and environmental impact, *Geoph. Monog.*, 134,  
348 1–35, 2003.

349 Johnsen, S. J., Dahl-Jensen, D., Gundestrup, N., Steffensen, J. P., Clausen, H. B., Miller, H., Masson-  
350 Delmotte, V., Sveinbjörnsdóttir, A. E., and White, J.: Oxygen isotope and palaeotemperature  
351 records from six Greenland ice-core stations: Camp Century, Dye-3, GRIP, GISP2, Renland and  
352 NorthGRIP, *J. Quaternary Sci.*, 16, 299–307, 2001.

353 Josey, S. A., Somot, S., and Tsimplis, M.: Impacts of atmospheric modes of variability on  
354 Mediterranean Sea surface heat exchange, *J. Geophys. Res.-Oceans*, 116, C02032,  
355 doi:10.1029/2010JC006685, 2011.

356 Kallel, N., Paterne, M., Duplessy, J.C., Vergnaud-Grazzini, C., Pujol, C., Labeyrie, L., Arnold, M.,  
357 Fontugne, M., Pierre, C.: Enhanced rainfall in the Mediterranean region during the last sapropel  
358 event, *Oceanologica Acta*, 20, 697–712, 1997a.

359 Kallel, N., Paterne, M., Labeyrie, L., Duplessy, J.C., Arnold, M.: Temperature and salinity records of  
360 the last 18 000 years, *Palaeogeogr., Paleoclimatol., Paleoecol.*, 135, 97–108, 1997b.

361 Kallel, N., Duplessy, J.C., Labeyrie, L., Fontugne, M., Paterne, M.: Mediterranean Sea  
362 palaeohydrology and pluvial periods during the Late Quaternary. In: Battarbee, R.W., Gasse, F.,  
363 Stickley, C.E. (Eds.), *Past climate variability through Europe and Africa*, Kluwer Academic,  
364 Dordrecht, 6, 307–324, 2004.

365 Kushnir, Y. and Stein, M.: North Atlantic influence on 19th–20th century rainfall in the Dead Sea  
366 watershed, teleconnections with the Sahel, and implication for Holocene climate fluctuations,  
367 *Quaternary Sci. Rev.*, 29, 3843–3860, 2010.

368 Ludwig, W., Bouwman, A. F., Dumont, E., and Lespinas, F.: Water and nutrient fluxes from major  
369 Mediterranean and Black Sea rivers: past and future trends and their implications for the basin  
370 scale budgets, *Global Biogeochem. Cy.*, 24, GB0A13, doi:10.1029/2009GB003594, 2010.

371 Marcott, S. A., Shakun, J. D., Clark, P. U., and Mix, A. C.: A reconstruction of regional and global  
372 temperature for the past 11 300 years, *Science*, 339, 1198–1201, 2013.

373 Martrat, B., Jimenez-Amat, P., Zahn, R., and Grimalt, J.-O.: Similarities and dissimilarities between the  
374 last two deglaciations and interglaciations in the North Atlantic region, *Quaternary Sci. Rev.*, 99,  
375 122–134, doi:10.1016/j.quascirev.2014.06.016, 2014.

376 Mayewski, P. A., Rohling, E. E., Stager, J. C., Karlen, W., Maasch, K. A., Meeker, L. D., Meyerson, E.  
377 A., Gasse, F., van Kreveld, S., Holmgren, K., Lee-Thorp, J., Rosqvist, G., Rack, F., Staubwasser,  
378 M., Schneider, R. R., and Steig, E. J.: Holocene climate variability, *Quaternary Res.*, 62, 243–255,  
379 2004.

380 Millot, C.: Circulation in the Western Mediterranean Sea, *J. Marine Syst.*, 20, 423–442, 1999.

381 Müller, P. J., Kirst, G., Ruthland, G., von Storch, I., and Rosell-Melé, A.: Calibration of the alkenone  
382 paleotemperature index UK'37 based on core-tops from the eastern South Atlantic and the global  
383 ocean (60N-60S), *Geochim. Cosmochim. Ac.*, 62, 1757–1772, 1998.

384 Olsen, J., Anderson, N. J., and Knudsen, M. F.: Variability of the North Atlantic Oscillation over the  
385 past 5200 years, *Nat. Geosci.*, 5, 808–812, 2012.

386 Provansal, M., Vella, C., Arnaud-Fassetta, G., Sabatier, F., and Maillet, G.: Role of fluvial sediment  
387 inputs in the mobility of the Rhône delta coast (France), *Geomorphologie*, 4, 271–282, 2003.

388 Ramsey, C.-B. and Lee, S.: Recent and planned developments of the program OxCal, *Radiocarbon*,  
389 55, 720–730, 2013.

390 Reimer, P. J., Bard, E., Bayliss, A., Beck, J. W., Blackwell, P. G., Bronk Ramsey, C., Grootes, P. M.,  
391 Guilderson, T. P., Hafflidason, H., Hajdas, I., Hatt, C., Heaton, T. J., Homann, D. L., Hogg, A. G.,  
392 Hughen, K. A., Kaiser, K. F., Kromer, B., Manning, S. W., Niu, M., Reimer, R. W., Richards, D. A.,  
393 Scott, E. M., Southon, J. R., Staff, R. A., Turney, C. S. M., and van der Plicht, J.: IntCal13 and  
394 Marine13 Radiocarbon Age Calibration Curves 0–50 000 years cal BP, *Radiocarbon*, 55, 1869–  
395 1887, 2013.

396 Rimbu, N., Lohmann, G., Kim, J.-H., Arz, H. W., and Schneider, R.: Arctic/North Atlantic oscillation  
397 signature in holocene sea surface temperature trends as obtained from alkenone data, *Geophys.*  
398 *Res. Lett.*, 30, 1280, doi:10.1029/2002GL016570, 2003.

399 Rohling, E. J., Mayewski, P. A., Abu-Zied, R. H., Casford, J. S. L., and Hayes, A.: Holocene  
400 atmosphere–ocean interactions: records from Greenland and the Aegean Sea, *Clim. Dynam.*, 18,  
401 587–593, doi:10.1007/s00382-001-0194-8, 2002.

402 [Schimmelpfennig, I., Schaefer, J.-M., Akçar, N., Ivy-Ochs, S., Finkel, R.-C., and Schlüchter, C.:](#)  
403 [Holocene glacier culminations in the Western Alps and their hemispheric relevance, \*Geology\*, 40,](#)  
404 [891–894, 2012.](#)

405 Schroeder, K., Borghini, M., Cerrati, G., Difesca, V., Delfanti, R., Santinelli, C., and Gasparini, G. P.:  
406 Multiparametric mixing analysis of the deep waters in the western Mediterranean Sea, *Chem.*  
407 *Ecol.*, 24, 47–56, 2008.

408 Schroeder, K., Josey, S. A., Herrmann, M., Grignon, L., Gasparini, G. P., and Bryden, H. L.: Abrupt  
409 warming and salting of the Western Mediterranean Deep Water after 2005: atmospheric forcings  
410 and lateral advection, *J. Geophys. Res.*, 115, C08029, doi:10.1029/2009JC005749, 2010.

411 Schroeder, K., Haza, A. C., Griffa, A., Özgökmen, T. M., Poulain, P., Gerin, R., Peggion, G., and  
412 Rixen, M.: Relative dispersion in the liguro-provencal basin: from sub-mesoscale to mesoscale,  
413 *Deep-Sea Res. Pt. I*, 58, 861–882, 2011.

414 Sicre, M.-A., Martrat, B., Jalali, B., Schmidt, S., Bassetti, M.-A., and Kallel, N.: Sea surface  
415 temperature variability in the North Western Mediterranean Sea (Gulf of Lions) during the Common  
416 Era, *Earth Planet. Sc. Lett.*, revised, 2015.

417 Stuiver, M. and Reimer, P. J.: Extended 14C database and revised CALIB 3.0 14C age calibration  
418 program, *Radiocarbon*, 35, 215–230, 1993.

419 Ternois, Y., Sicre, M.-A., Boireau, A., Marty, J.-C., and Miquel, J.-C.: Production pattern of alkenones  
420 in the Mediterranean Sea, *Geophys. Res. Lett.*, 23, 3171–3174, 1996.

421 [Trigo, I.-F., and Davies, T.-D.: Decline in Mediterranean rainfall caused by weakening of](#)  
422 [Mediterranean cyclones, \*Geophys. Res. Lett.\*, 27, 2913-2916, 2000.](#)

423 Trouet, V., Esper, J., Graham, N. E., Baker, A., Scourse, J. D., and Frank, D. C.: Persistent positive  
424 North Atlantic oscillation mode dominated the medieval climate anomaly, *Science*, 324, 78–80,  
425 2009.

426 Wanner, H., Solomina, O., Grosjean, M., Ritz, S. P., and Jetel, M.: Structure and origin of Holocene  
427 cold events, *Quaternary Sci. Rev.*, 30, 3109–3123, 2011.

428 Wanner, H., Mercolli, L., Grosjean, M., and Ritz, S. P.: Holocene climate variability and change; a  
429 data-based review, *J. Geol. Soc. London*, 172, 254–263, doi:10.1144/jgs2013-101, 2014.

430 Wirth, S. B., Glur, L., Gilli, A., and Anselmetti, F. S.: Holocene flood frequency across the Central Alps  
431 – solar forcing and evidence for variations in North Atlantic atmospheric circulation, *Quaternary Sci.*  
432 *Rev.*, 80, 112–128, doi:10.1016/j.quascirev.2013.09.002, 2013.

433

434 Table 1. AMS radiocarbon dated levels and their calibrated ages with a 1  $\sigma$  uncertainty for the  
 435 KSGC-31 gravity core. The analyses were performed at the Laboratoire de Mesure du  
 436 Carbone 14, Saclay (France) and at the Beta Analytic Radiocarbon Dating Laboratory  
 437 (Florida; USA). Raw radiocarbon  $^{14}\text{C}$  ages were corrected and calibrated to calendar ages  
 438 using the Calib7.1 software (Stuiver and Reimer, 1993) and the MARINE13 calibration  
 439 dataset (Reimer et al., 2013).

440

Depth (cm)	Material	Radiocarbon age $\pm 1$ error (yr BP)	Calibrate Age (cal BP)	$\pm 1$ error
5.5	Bittium sp.	420 $\pm$ 30	24 <sup>a</sup>	60
11.5	Tellina sp.	430 $\pm$ 30	34 <sup>a</sup>	60
18.5	Pecten sp.	720 $\pm$ 40	350 <sup>b</sup>	78
25.5	Venus sp.	640 $\pm$ 30	234	99
41	Pecten sp.	700 $\pm$ 30	339	79
52	Indet. bivalve	960 $\pm$ 30	551	59
71	Arca tetragona	1340 $\pm$ 30	851	80
110.5	Venus sp.	1465 $\pm$ 30	992	85
186.5	Nucula sp.	2235 $\pm$ 40	1805	99
251	Juvenile bivalve shells (ind.)	2940 $\pm$ 30	2674	100
330.5	Venus cosina	3870 $\pm$ 30	3796	106
370.5	Nuculana sp.	4170 $\pm$ 30	4223	113
390.5	Turritella sp.	4500 $\pm$ 30	4676	106
460	Venus sp.	5530 $\pm$ 45	5873	106
481	Ostrea sp.	5955 $\pm$ 35	6348	78
501.5	Turritella sp.	6380 $\pm$ 50	6826	107
552	coquilles	7215 $\pm$ 30	7653	75
583	Turritella sp.	7860 $\pm$ 60	8288	92
652	Turritella sp.	8310 $\pm$ 35	8843	121
700.5	Turritella sp.	9215 $\pm$ 30	10006	123
701	Turritella sp.	9190 $\pm$ 50	9968	145

441

442 <sup>a</sup> post-bomb radiocarbon ages, obtained using OxCal 4.2 (Ramsey and Lee, 2013), not used  
 443 for the interpolation.

444 <sup>b</sup> Reversal date, not used for the interpolation.

445

446

447

448

449

450

451

452

453

454 Table 2: Timing of Holocene cold relapses (CRs). Age uncertainty was estimated using a  
 455 Bayesian approach of OxCal 4.2. The cooling amplitudes were determined by the difference  
 456 between temperature at the beginning of CR and the lowest value after applying a 60 yr FFT  
 457 smoothing.

458

Cold relapses	Central Age year BP $\pm$ 1 uncertainty	Age interval year BP	Duration year	Amplitude $^{\circ}$ C
CR1	6175 $\pm$ 133	6600 - 5750	850	1.3 $\pm$ 0.3
CR2	5195 $\pm$ 196	5350 - 5040	310	1.3 $\pm$ 0.3
CR3	4130 $\pm$ 126	4340 - 3920	420	2.4 $\pm$ 0.3
CR4	2355 $\pm$ 142	2530 - 2180	350	1.4 $\pm$ 0.3
CR5	1365 $\pm$ 119	1770 - 960	810	2 $\pm$ 0.3
CR6	320 $\pm$ 75	490 - 150	340	1.1 $\pm$ 0.3

459

460

461 Table 3: Timing of High TEER-alkane episodes (HTE). Age uncertainty was estimated using  
 462 a Bayesian approach of OxCal 4.2. HTE were defined as the time span where values exceed  
 463 one half of the standard deviation of the Holocene mean value after applying a 60 yr FFT  
 464 smoothing. Amplitudes were determined by the difference between highest TERR-alkanes  
 465 and the value at the beginning of HTE.

466

High TERR-alkanes episodes	Central Age year BP $\pm$ 1 uncertainty	Age interval year BP	Duration year	Amplitude ng/g
HTE1	5995 $\pm$ 135	5235 - 4755	480	388
HTE2	4045 $\pm$ 126	4330 - 3760	570	440
HTE3	3425 $\pm$ 172	3520 - 3330	190	348
HTE4	3020 $\pm$ 181	3195 - 2845	350	466
HTE5	1390 $\pm$ 115	1565 - 1215	350	335
HTE6	832 $\pm$ 64	1090 - 575	515	875
HTE7	221 $\pm$ 100	416 - 26	390	400

467 Table 4. List of data sets used in Figure 3.

468

Location / Core	Proxy	Temperature Calibration/ Reference	Latitude (°)	Longitude (°)	Elevation (m)	Resolution (yr)	Reference
ODP Site 161-976	UK'37	Müller et al., 1998	36.20	-4.31	-1108	34	Martrat et al., 2014
MD95-2043	UK'37	Müller et al., 1998	36.10	-2.60	-1000	110	Cacho et al., 2001
KSGC-31_GolHo-1B	UK'37	Conte et al., 2006	43.00	3.29	-60	14	This study
MD99-2343	$\delta^{18}\text{O}$ (G. bulloides)	-	40.49	4.02	-2391	110	Frigola et al., 2007
BS79-38	UK'37	Müller et al., 1998	38.41	13.57	-1489	59	Cacho et al., 2001
AD91-17	UK'37	Müller et al., 1998	40.90	18.60	-844	190	Giunta et al., 2001
M25/4-KL11	UK'37	Müller et al., 1998	36.70	17.70	-3376	260	Emeis et al., 2003
M40/4-SL78	UK'37	Müller et al., 1998	37.03	13.18	-467	160	Emeis et al., 2003
MD 99-917	UK'37	Conte et al., 2006	41.28	17.61	-1010	40	Essallami et al., 2007
GeoB 7702-3	TEX86 UK'37	Kim et al., 2008 Müller et al., 1998	31.7	34.1	-562	210	Castañeda et al., 2010
ODP Site 160-967D	UK'37	Müller et al., 1998	34.07	32.72	-2552	94	Emeis et al., 2000

469

470 **Figure captions**

471

472 Figure 1. Map of the Mediterranean annual mean SSTs (°C) (1955 and 2012) from Word Ocean Atlas  
473 2013 ([http://odv.awi.de/de/data/ocean/world\\_ocean\\_atlas\\_2013/](http://odv.awi.de/de/data/ocean/world_ocean_atlas_2013/)) plotted using Ocean Data View  
474 (Brown, 1998). The location of the KSGC-31\_GolHo-1B core and other sites discussed in the text are  
475 also reported (from West to East): ODP Site 161-976, Alboran Sea (Martrat et al., 2014); MD95-2043,  
476 Alboran Sea (Cacho et al., 2001); MD 99-2343, Balearic basin (Frigola et al., 2007); M40/4-SL78,  
477 Ionian Sea (Emeis et al., 2003); BS79-38, Southern Tyrrhenian Sea (Cacho et al., 2001); MD90-917,  
478 Southern Adriatic Sea (Essallami et al., 2007); M25/4-KL11, the Ionian Sea (Emeis et al., 2003);  
479 AD91-17, Southern Adriatic Sea (Giunta et al., 2001); ODP Site 160-967D, Levantine basin (Emeis et  
480 al., 2000); GeoB 7702-3, Levantine basin (Castañeda et al., 2010). The location of Lake Bourget in  
481 France (LDB01-1 and LDB04-1 cores) is also shown (Arnaud et al., 2012). The main winds blowing  
482 in the Mediterranean Sea are shown by red arrows.

483

484 Figure 2. Alkenone SSTs and TERR-alkane concentrations at the KSGC-31\_GolHo-1B core site over  
485 the past 10000 years. (a) The AMS <sup>14</sup>C radiocarbon dates for gravity core KSGC-31 are indicated by  
486 the blue diamonds; vertical dashed lines highlight the major periods of the Common Era. (b) TERR-  
487 alkane concentrations. (c) The UP10 fraction from core MD99-2343 (Frigola et al., 2007), (reversed  
488 vertical axis). Age control points for core MD99-2343 are represented by the purple diamonds. The  
489 vertical gray bars represent the six NW Mediterranean CRs no. 1-6. Vertical light brown bars indicate  
490 the periods of high flood intensity based on the high TERR-alkane peaks.

491

492 Figure 3. SST records in the Mediterranean Sea over the Holocene. (a) Core MD95-2043 from the  
493 Alboran Sea (Cacho et al., 2001). (b) ODP Site 161-976 from the Alboran Sea (Martrat et al., 2014).  
494 (c) Core KSGC-31\_GolHo-1B from the Gulf of Lions (this study). (d) G. bulloides oxygen isotopic  
495 record for core MD99-2343 from the Balearic Sea (Frigola et al., 2007). (e) Core BS79-38 from the  
496 Southern Tyrrhenian Sea (Cacho et al., 2001). (f) Core AD91-17 from the Adriatic Sea (Giunta et al.,  
497 2001). (g) Core M25/4-KL11 from the Ionian Sea (Emeis et al., 2003). (h) Core M40/4-SL78 from the  
498 Ionian Sea (Emeis et al., 2003). (i) Core MD90-917 from the Southern Adriatic Sea (Essallami et al.,  
499 2007). (j) Core GeoB 7702-3 from the Levantine basin (Castañeda et al., 2010). (k) ODP Site 160-  
500 967D from the Levantine basin (Emeis et al., 2000). Vertical grey bars represent the time interval of  
501 the CRs, no. 1-6. The grey vertical dashed lines indicate the time interval used to calculate SST trends  
502 (7000 to 1000 yrs BP). SST trends between 7000 and 1000 yrs are marked by arrows and the  
503 amplitudes (°C/6 kyr) are indicated in the right of each curve.

504

505 Figure 4. Holocene flood changes in the NW Mediterranean Sea and Alps region. (a) TERR-alkane  
506 abundances as a proxy of flood intensity. (b) Flood activity in the North and South Alps (from Wirth  
507 et al., 2013). (c) Total terrigenous fraction (%) indicates the Rhone river discharge into lake Bourget  
508 (Arnaud et al., 2012) (green curve). (d) The UP10 fraction from core MD99-2343 (Frigola et al., 2007)  
509 (purple curve) and the winter-NAO index from Trouet et al. (2009) (in red) and Olsen et al. (2012) (in  
510 blue). Vertical light brown bars indicate the periods of high flood intensity based on the high TERR-  
511 alkane peaks.

# World Ocean Atlas 2013 (1955-2012 SST)

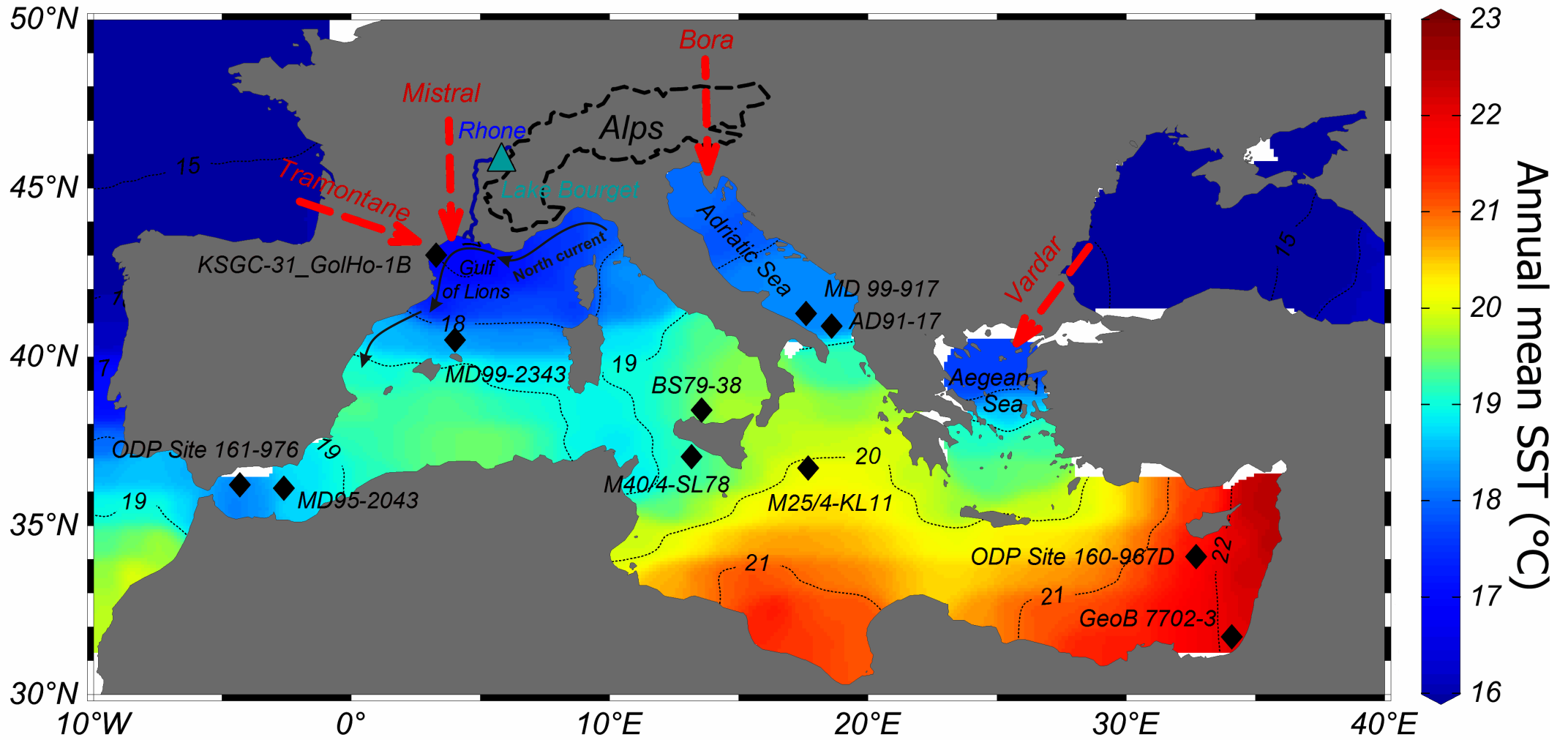


Figure 1

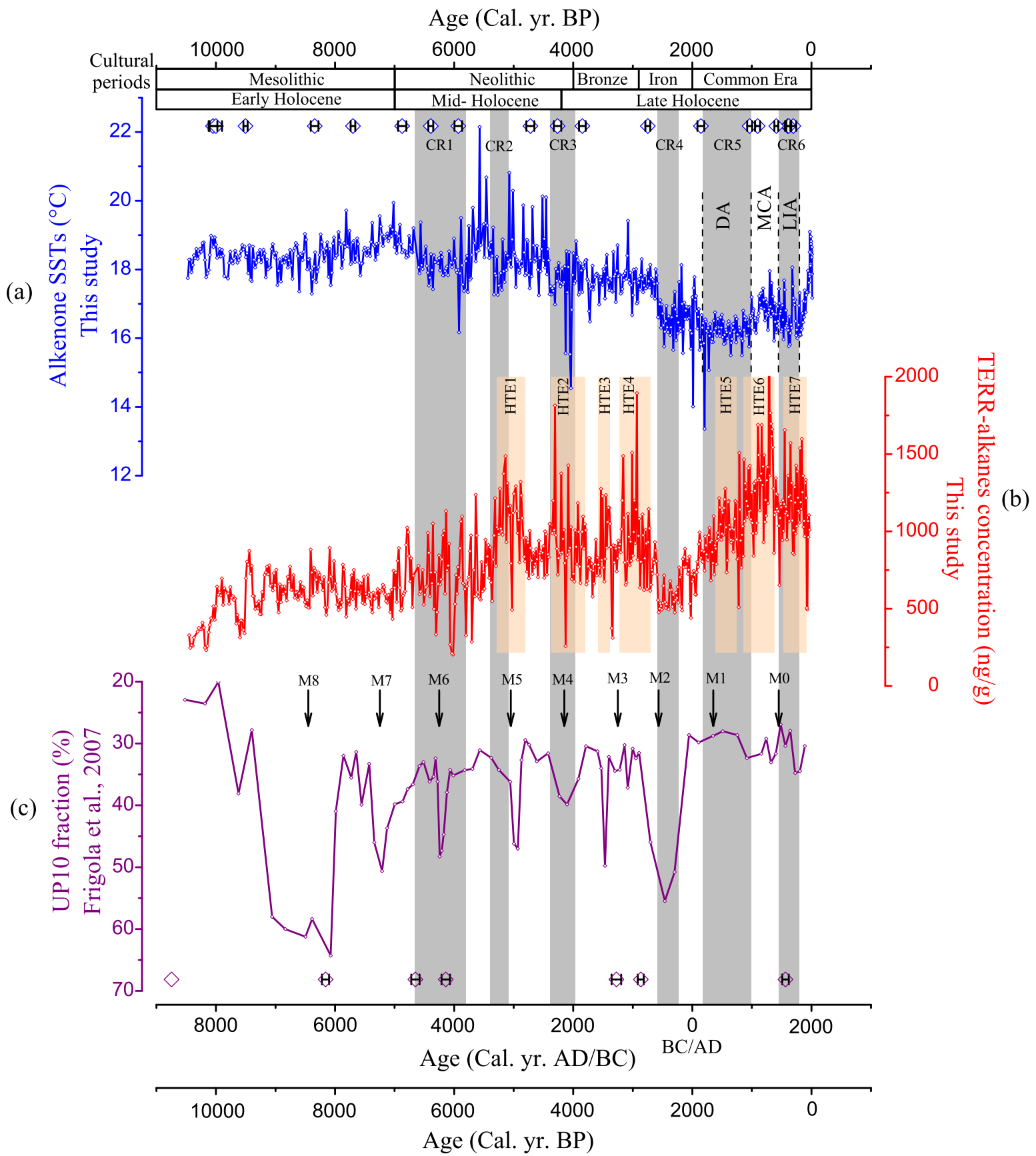


Figure 2

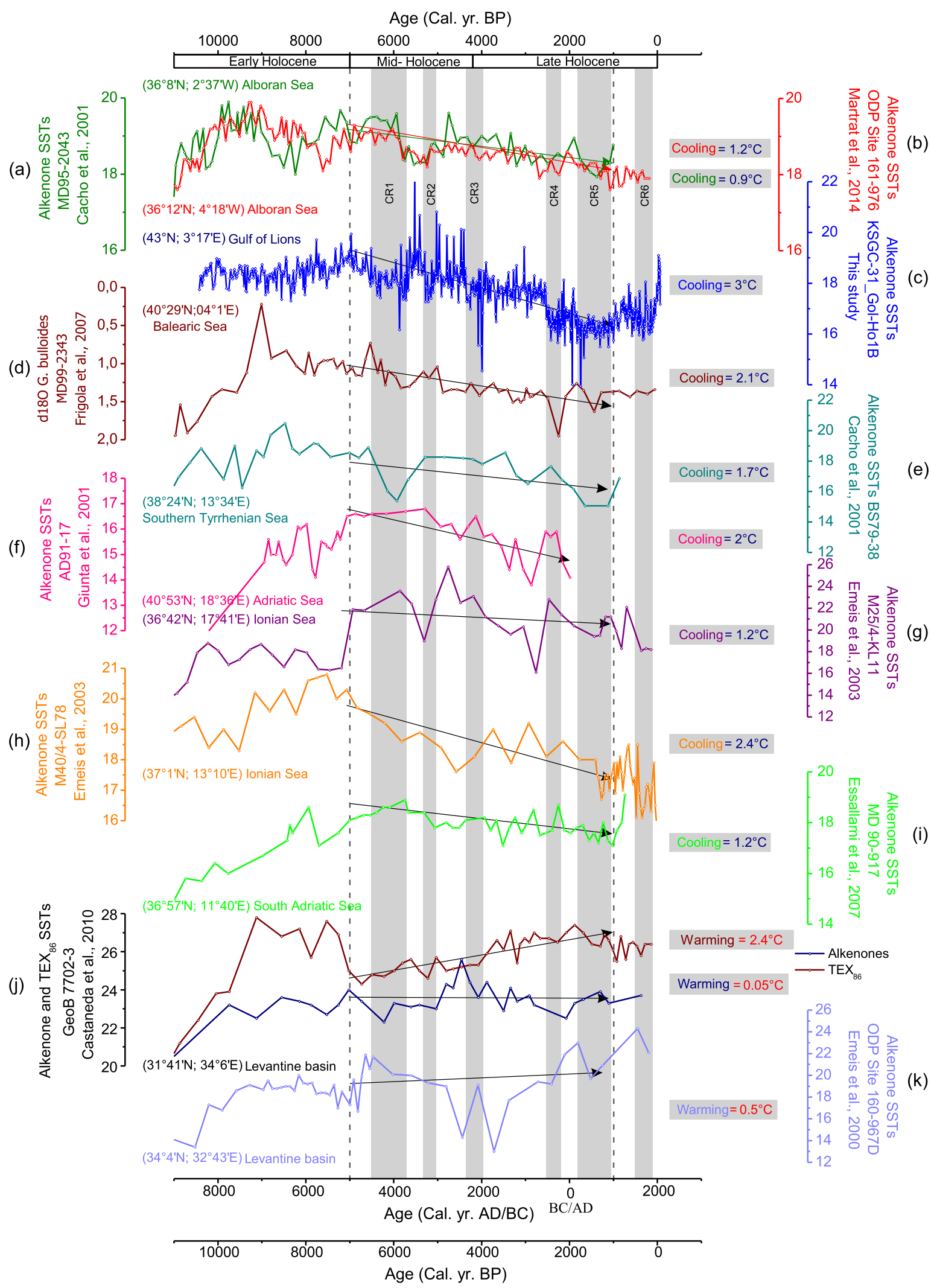


Figure 3

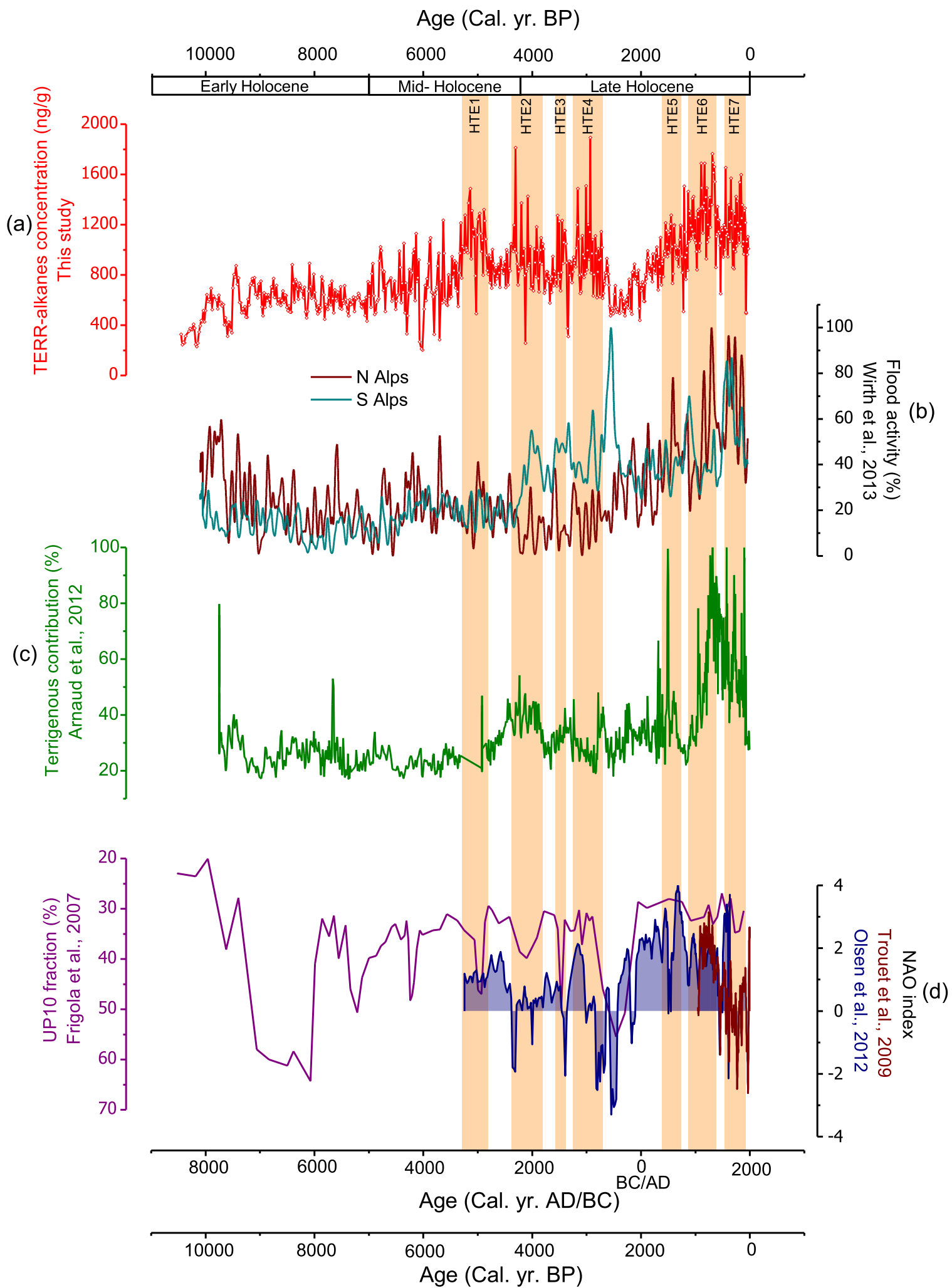


Figure 4